X-ray radiation damage effects on double-SOI pixel detectors for the future astronomical satellite FORCE

Masatoshi Kitajima,[a] Kouichi Hagino[a,b,*] Takayoshi Kohmura,[a] Mitsuki Hayashida,[a] Kenji Oono,[a] Kousuke Negishi,[a] Keigo Yarita,[a] Toshiki Doi,[a] Shun Tsunomachi,[a] Takeshi G. Tsuru,[c] Hiroyuki Uchida,[c] Kazuho Kayama,[c] Ryota Kodama,[c] Takaaki Tanaka,[d] Koji Mori,[e] Ayaki Takeda,[e] Yusuke Nishioka,[e] Masataka Yukumoto,[e] Kira Mieda,[e] Syuto Yonemura,[e] Tatsunori Ishida,[e] Yasuo Arai,[f] and Ikuo Kurachi[g]

[a]Tokyo University of Science, School of Science and Technology, Department of Physics, Noda, Japan
[b]Kanto Gakuin University, Research Advancement and Management Organization, Yokohama, Japan
[c]Kyoto University, Department of Physics, Faculty of Science, Kyoto, Japan
[d]Konan University, Department of Physics, Kobe, Japan
[e]University of Miyazaki, Department of Applied Physics, Faculty of Engineering, Miyazaki, Japan
[f]Institute of Particle and Nuclear Studies, High Energy Accelerator Research Organization (KEK), Tsukuba, Japan
[g]D&S Inc., Tokyo, Japan

Abstract. We have been developing the monolithic active pixel detector XRPIX onboard the future x-ray astronomical satellite FORCE. XRPIX is composed of complementary metal-oxide-semiconductor pixel circuits, SiO_2 insulator, and Si sensor by utilizing the silicon-on-insulator (SOI) technology. When the semiconductor detector is operated in orbit, it suffers from radiation damage due to x-rays emitted from celestial objects as well as cosmic rays. From previous studies, positive charges trapped in the SiO_2 insulator are known to cause degradation of the detector performance. To improve the radiation hardness, we developed XRPIX equipped with a double-SOI (D-SOI) structure, introducing an additional silicon layer in the SiO_2 insulator. This structure is aimed at compensating for the effect of the trapped positive charges. Although the radiation hardness of the D-SOI detectors to cosmic rays has been evaluated, the radiation effect due to x-ray irradiation has not been evaluated. Thus, we then conduct an x-ray irradiation experiment using an x-ray generator with a total dose of 10 krad at the SiO_2 insulator, equivalent to 7 years in orbit. As a result of this experiment, the energy resolution in full-width half maximum for the 5.9 keV x-ray degrades by $17.8\% \pm 2.8\%$ and the dark current increases by $89\% \pm 13\%$. We also investigate the physical mechanism of the increase in the dark current due to x-ray irradiation using technology computer-aided design simulation. It is found that the increase in the dark current can be explained by the increase in the interface state density at the Si/SiO_2 interface. © *The Authors. Published by SPIE under a Creative Commons Attribution 4.0 International License. Distribution or reproduction of this work in whole or in part requires full attribution of the original publication, including its DOI.* [DOI: 10.1117/1.JATIS.8.2.026007]

1 Introduction

Since the 1990s, the charge-coupled device (CCD) has been the standard detector used in x-ray astronomy satellites. The x-ray CCD has an excellent position and energy resolution; however,

---

*Address all correspondence to Kouichi Hagino, hagino@kanto-gakuin.ac.jp

it has a poor time resolution of a few seconds and a narrow observable energy band of 0.3 to 10 keV. To realize broadband and high-sensitivity x-ray observation, we have been developing the monolithic active pixel detector XRPIX onboard the future x-ray astronomical satellite FORCE.[1,2] FORCE will be equipped with two x-ray supermirrors, with angular resolution that will be better than 15″ in half-power diameter. The focal plane detector is composed of two stacks of Si sensors (XRPIX) and CdTe sensors, and these detectors cover the x-ray energy ranging from 1 to 79 keV. XRPIX is composed of complementary metal-oxide-semiconductor (CMOS) pixel circuits, the SiO_2 insulator called the buried oxide (BOX) layer, and the Si sensor by utilizing the silicon-on-insulator (SOI) technology.[3] This makes it possible to implement Si with low and high resistivity in the circuit and sensor layers, respectively. Because the sensor layer has high resistivity, the depletion layer thickness can be a few hundreds of micrometers. In addition, the CMOS circuit in each pixel has a self-trigger function, so only the pixels for which an x-ray is incident can be read out, achieving a time resolution of <10 μs.

XRPIX will suffer from radiation damage due to the irradiation of bright x-rays from compact stars as well as high-energy cosmic rays. When the detector is irradiated by charged particles or x-rays, electron-hole pairs are produced in Si and in SiO_2. In the former case, carriers are collected by electrodes. On the other hand, in the SiO_2 insulator, electrons are immediately collected to electrodes, but some parts of holes are trapped there because of their low mobility μ_h compared with that of electrons μ_e ($\mu_h/\mu_e \sim 10^{-10}$ at 300 K).[4] It is known that the trapped positive charges in the SiO_2 insulator cause a shift of threshold voltages of CMOS pixel circuits and degradation of the detector performance.[5]

To improve the radiation hardness, we introduce a double-SOI (D-SOI) structure, which has an additional Si layer called "middle-Si" in the SiO_2 insulator, as shown in Fig. 1. It is effective against radiation damage because the negative voltage applied on the middle-Si negates the effect of trapped positive charges in the SiO_2 insulator caused by radiation exposure.[6]

In a prior experiment, to evaluate the effect of cosmic rays mainly composed of high energy protons, we evaluated the radiation hardness of the D-SOI detector by 6-MeV proton beam irradiation.[6] In this experiment, we found that, even after irradiation of ~5 krad, degradation of the energy resolution was as small as 7%. Moreover, we found that the gain degradation can be quantitatively explained by the sense-node capacitance increased by the trapped positive charges. On the other hand, because high-energy x-rays up to 79 keV emitted from celestial objects are focused with x-ray supermirrors at the focal point with a high angular resolution of <15″, the focused high-energy x-rays can cause serious radiation damage against XRPIX.[7] Thus, in this paper, we conduct an x-ray irradiation experiment to evaluate the x-ray radiation hardness of the D-SOI detector.[8] The x-ray irradiation experiment is described in Sec. 2, and we show its results in Sec. 3. In Sec. 4, we discuss the possible cause of the degradation of detector performance, mainly regarding the dark current using device simulation. Section 5 provides the conclusions of this study.
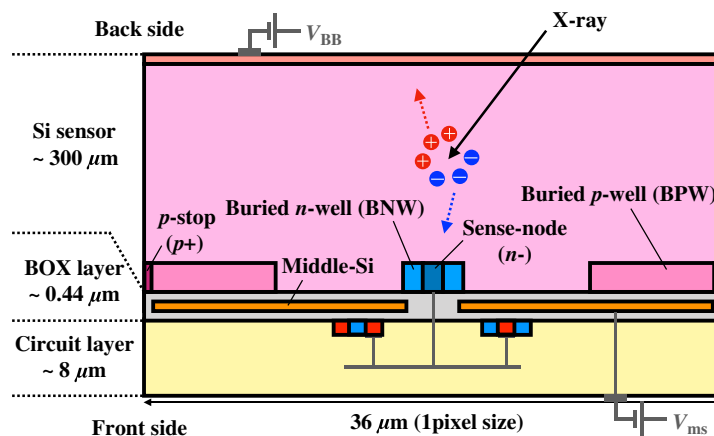

Fig. 1 Schematic cross-sectional view of XRPIX6C with D-SOI structure.

Table 1 The chip design of XRPIX6C.

Parameter	Value
Chip size	4.45 mm × 4.45 mm
Sensor area	1.7 mm × 1.7 mm
Pixel size	36 μm × 36 μm
Number of pixels	48 × 48
Thickness of sensor	300 μm
Type of sensor layer	Froating zone p-type Si
Sensor resistivity	4 kΩ cm

2 X-Ray Irradiation Experiment

We conducted an x-ray irradiation experiment on D-SOI detector, called XRPIX6C. Figure 1 and Table 1 show the schematic cross-sectional structure and chip design of XRPIX6C, respectively. The sensor layer, with a thickness of 300 μm, is p-type Si bulk, and its resistivity is 4 kΩ cm. With this thickness, the back-bias voltage V_{BB} should be higher than $\simeq -216$ V for full depletion. In this experiment, we applied a back-bias voltage $V_{BB} = -250$ V. In this device, each pixel is isolated from each other by a p-stop and has a sense node surrounded by a buried n-well (BNW). BNW was introduced to prevent interference between the sensor layer and the circuit layer.[9] A buried p-well (BPW) was introduced to generate a lateral electric field structure from the pixel boundary to the sense node so that electric charges collect at the sense node. It is also effective in suppressing dark current by covering the Si/SiO$_2$ interface. We call this device D-SOI because an additional Si layer called middle-Si is introduced in the BOX layer. It compensates for the effect of positive charges trapped in the BOX layer by biasing negatively. We applied a negative voltage of -2.5 V to middle-Si during the experiment.

Figure 2 shows the schematic view of our experimental setup. XRPIX6C was installed in a vacuum chamber and cooled down to $\simeq -65°$C to reduce the shot noise of the dark current. We irradiated x-rays on the back side (sensor layer side; see Fig. 1) of XRPIX6C using an x-ray tube (Mini-X2, AMPTEK) attached to the vacuum chamber. The x-ray tube was operated at 20 kV with a target of Au. The energies of L-shell fluorescence lines of Au are 9.7 keV (L_α), 11.4 keV (L_β), and 13.4 keV (L_γ). XRPIX6C was irradiated with x-ray to a total dose of 10 krad at the BOX layer. Assuming that we observe the Crab Nebula, one of the observational targets of FORCE, for 100 ksec per month based on a previous study,[7] 10 krad corresponds to 7 years of in-orbit operation.
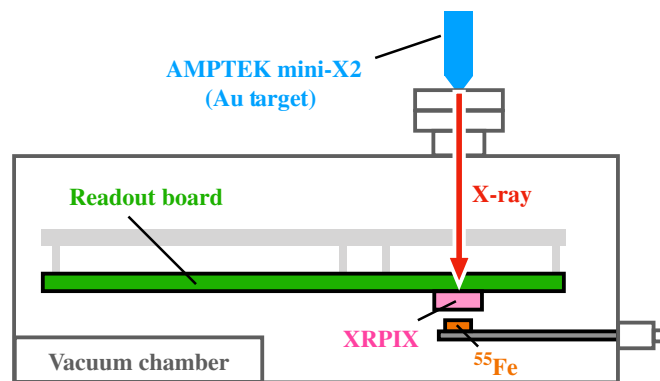

Fig. 2 Schematic view of experimental setup. We irradiated x-rays on the back side of XRPIX using an x-ray tube and irradiated x-rays of ^{55}Fe on the front side to evaluate the performance of XRPIX.

The degradation of the detector performance was monitored by iterating the x-ray irradiation and data acquisition of ^{55}Fe. These evaluation data were taken after irradiations of 0.1, 0.5, 1, 2, 4, 7, and 10 krad. To avoid the large dark current after the irradiation, the evaluations were performed after the dark current settled down to steady values.

3 Results of Irradiation Experiment

We evaluated the spectral performance of XRPIX by irradiating x-rays of the ^{55}Fe radioisotope from the front side (circuit layer side). We took 5×10^5 frames of the x-ray data with a 1-ms integration time. Figure 3 shows the spectra of single-pixel events, which are extracted when a pulse height of one pixel exceeds the event threshold (100 ADU $\simeq$ 2.1 keV), whereas the pulse heights of the surrounding 8 pixels are below the split threshold (60 ADU $\simeq$ 1.3 keV). The horizontal axis is the uncorrected pulse heights in analog-to-digital unit (ADU), and the vertical axis is the number of counts. The tail structure on the low-energy side of the peak becomes noticeable as the dose increases. This is probably caused by the charge loss due to the increase in the interface trap at the Si/SiO_2 interface by x-ray irradiation.[10]

We also evaluated the conversion gain and energy resolution of XRPIX6C using the measured peak position and FWHM of the MnK_α line derived by fitting with the Gaussian function. Figures 4(a) and 4(b) show the gain and energy resolution as functions of the total dose, respectively. Both of them were almost constant up to 2 krad, but after that, they degraded with increasing dose. Although an outlier of the gain at 2 krad indicates a possibility of a nonlinear relation to the dose, we assume a linear relation for simplicity. After 10-krad irradiation, the gain and energy resolution degraded by 2.84% ± 0.34% and 17.8% ± 2.8% compared with that of nonirradiation, respectively.

Figures 5(a) and 5(b) show the dark current and readout noise as functions of the dose, respectively. To evaluate the dark current, we measured the pedestal levels as a function of the integration time by reading pulse heights from all of the pixels with integration times of 0.1, 1, 2, 4, 8, 16, and 32 ms. Although this measurement was performed under the irradiation of x-rays from ^{55}Fe, its count rate was much <0.1 count/frame/pixel, even with the longest integration time of 32 ms. Thus, the effect of x-ray events on the pedestal measurement was negligible. In this measurement, the longer the integration time is, the more charge is accumulated and the higher pedestal level is output. Thus, we estimated the relationship between the integration time and pedestal level as a linear function and evaluated the dark current from the slope of the function. In addition, we evaluated the readout noise by measuring the pedestal width of each pixel. As shown in Fig. 5, both of them increased in proportion to the dose. After 10-krad irradiation, the dark current and readout noise increased by 89% ± 13% and 12.4% ± 0.9% compared with that of nonirradiation, respectively.
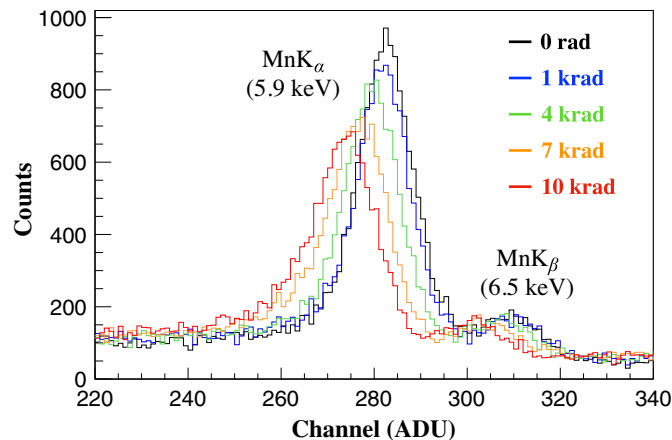

Fig. 3 ^{55}Fe energy spectra of XRPIX6C before and after x-ray irradiation. The horizontal axis is the uncorrected pulse heights in ADU, and the vertical axis is the number of counts.
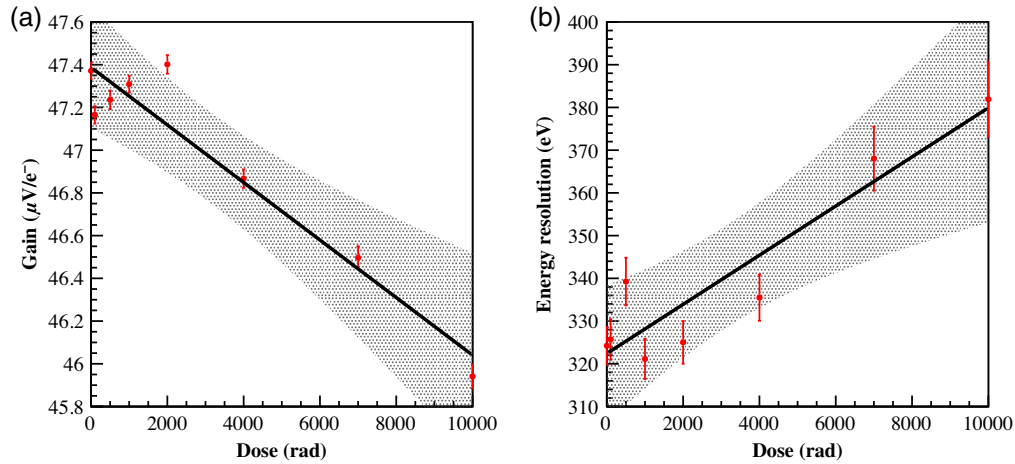
(a)

(b)

Fig. 4 (a) Conversion gain and (b) energy resolution of XRPIX6C as a function of dose level. Solid lines and shaded regions indicate the best fit linear functions and 95% confidence intervals, respectively. The confidence intervals are calculated on the assumption of Gaussian uncertainty of the data.
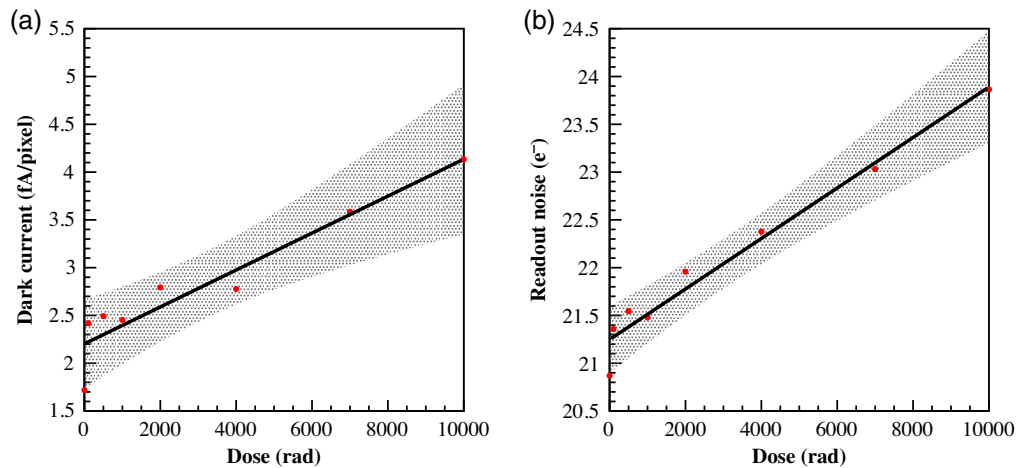
(a)

(b)

Fig. 5 (a) Dark current and (b) readout noise of XRPIX6C as a function of dose level. Best fit linear functions and 95% confidence intervals are overplotted similarly as in Fig. 4.

We also evaluated the fraction of "noisy pixels" to all pixels. The pixels above 3σ in the histogram of readout noise is judged to be noisy pixels. As shown in Fig. 6, there was little change from nonirradiation to 10 krad. Because the noisy pixels are not remarkably different from the normal pixels, the noisy pixels at 0 krad were not exactly the same pixels as those at 10 krad. As shown in Fig. 7, distributions of the readout noises in each pixel were almost the same shape with a slight shift. Therefore, these results suggest that there is an increase in noise on average, but no pixels show any extreme increase in noise.

4 Discussion

4.1 *Energy Resolution*

Figure 8 shows the ^{55}Fe energy spectra corrected for the gain degradation at 0 and 10 krad. The horizontal axis is the x-ray energy, and the vertical axis is the number of counts. In Fig. 8, the peak positions are aligned to focus on the change in spectral shape rather than the gain
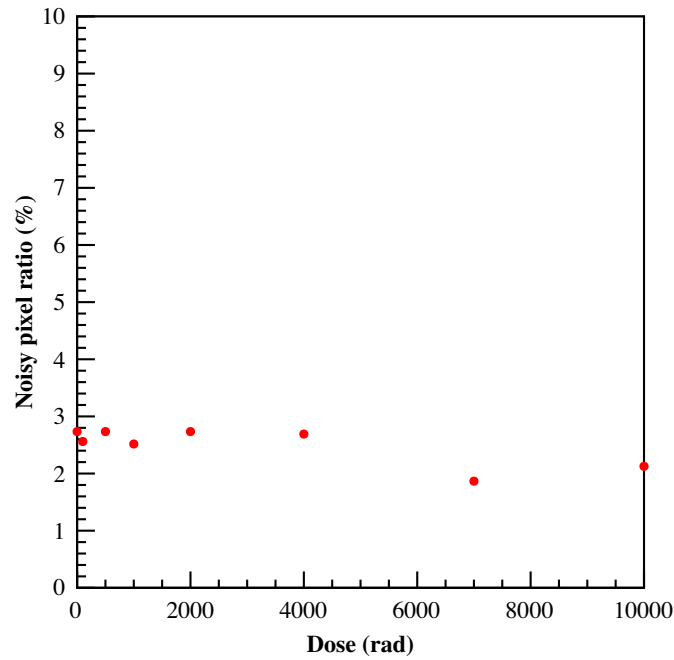
Fig. 6 Noisy pixel ratio of XRPIX6C as a function of dose level.
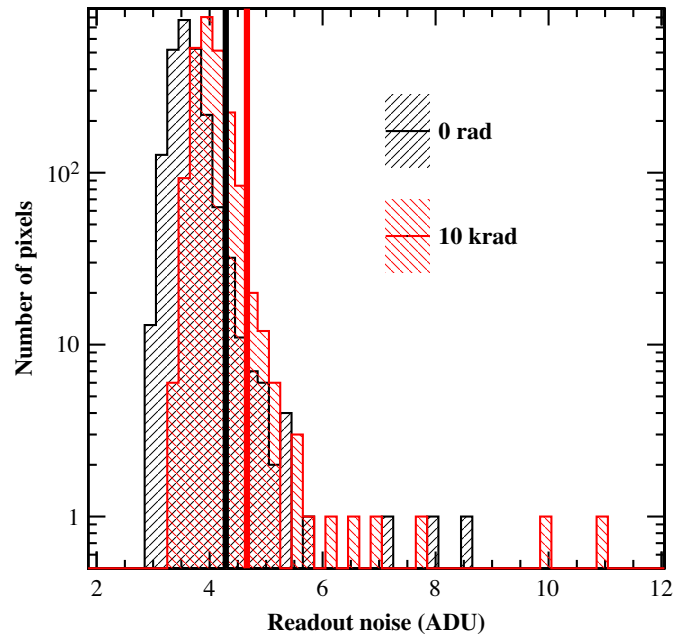

Fig. 7 Distributions of readout noise in each pixel of XRPIX6C before and after the x-ray irradiation. The noisy-pixel thresholds at $3 - \sigma$ are shown in black (0 rad) and red (10 krad) vertical thick solid lines.

degradation. The increase in the tail structure of the x-ray spectra was obviously observed after 10-krad irradiation. It contributes to the degradation of spectral performance.

This tail structure can be seen even before the irradiation, and we investigated this issue in a previous study.[10] This effect is likely caused by the charge loss at the Si/SiO_2 interface. When carriers generated in the sensor layer drift toward the sense-node along the electric field, they pass through the Si/SiO_2 interface, and some of them are captured in the trap level.
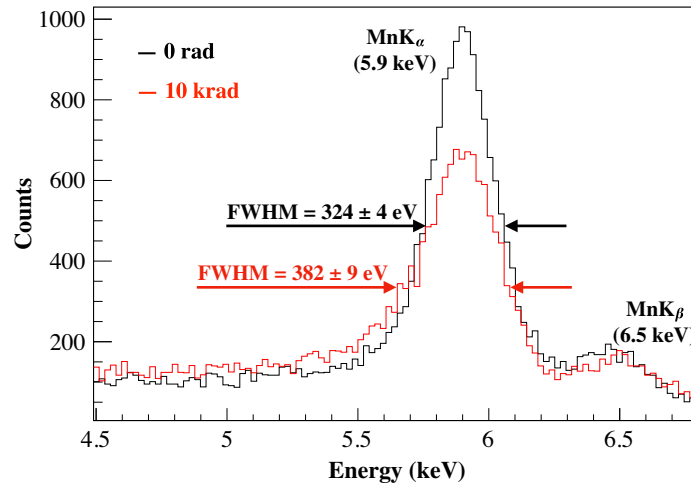
Fig. 8 ^{55}Fe energy spectra of XRPIX6C corrected for the gain degradation before and after x-ray irradiation. The horizontal axis is the x-ray energy, and the vertical axis is the number of counts. The tail structure increased at 10 krad compared with pre-irradiation.

As anticipated from prior studies, the interface state density increases due to radiation damage,[11] increasing the effects of charge loss and leading to an enlargement of the tail structure, as observed in Fig. 8.

4.2 Gain

The chip output gain is degraded by $2.84\% \pm 0.34\%$ after 10-krad irradiation. According to a previous study, the gain degradation due to radiation damage is caused by the enlargement of BNW.[6] This is explained by the effect of the positive charge trapped in the BOX layer due to x-ray irradiation. Its potential attracts electrons and enlarges the area of BNW. This phenomenon results in an increase in the sense node capacitance and the degradation of the gain. The relation between the inverse of the gain G and BNW size S_{BNW} is described in the previous study[6] as

$$\Delta\left(\frac{1}{G}\right) \simeq 3.4 \times 10^{-3} \times \left(\frac{\Delta S_{\mathrm{BNW}}}{1~\mu\mathrm{m}^2}\right)~\mathrm{fF}. \tag{1}$$

According to this equation, the change in the inverse of the gain $\Delta(1/G) \simeq 0.11$ fF after 10-krad irradiation is equivalent to the enlargement of BNW by $\Delta S_{\mathrm{BNW}} \simeq 31~\mu\mathrm{m}^2$. As the BNW width w_{BNW} is designed to be 3 μm, $w_{\mathrm{BNW}} \simeq \sqrt{3^2 + 31} \simeq 6.3~\mu$m at 10 krad. It is a reasonable value because the distance between BNW and BPW is designed to be 7 μm. In addition, it is considered that the charge loss at the Si/SiO$_2$ interface due to the increase in the interface state density contributed to the peak shift and caused the gain degradation.

4.3 Readout Noise

The readout noise increased by $12.4\% \pm 0.9\%$ after 10 krad irradiation. The gain degradation discussed in the previous section affects the increase of the readout noise. According to a previous study,[12] the readout noise σ in XRPIX is related to the gain G with an empirical relation of $\sigma \propto G^{-0.7}$. Therefore, the gain degradation of $\simeq 2.8\%$ after 10 krad contributes to the increase in the readout noise by $\simeq 2.2\%$. In addition, the increase in the shot noise due to the dark current increase also contributes to the increase in the readout noise. As the readout noise and dark current were evaluated using an integration time of 1 ms, the dark current increase of $\simeq 89\%$ after 10 krad contributes to the increase in the readout noise by $\simeq 1.7\%$. Therefore, it is assumed that the gain degradation and shot noise increase due to the increased dark current do not contribute significantly to the increase in the readout noise.

To solve the physical origin of readout noise increase, a more comprehensive analysis is needed. We are now formulating the readout noise due to the $1/f$ noise and thermal noise generated in the MOSFET in the main amplifier in each pixel circuit. In the radiation environment, the $1/f$ noise increases due to the increase in the interface trap.[13] Also, the increase in the sense-node capacitance[6] must affect the propagation of these $1/f$ and thermal noise. These full noise analyses will be our future work.

4.4 Dark Current

The dark current increased by $89\% \pm 13\%$ at 10 krad due to x-ray irradiation. We investigated its physical mechanism using technology computer-aided design (TCAD) device simulator HyDeLEOS, which is a part of the HyENEXSS.[14] In the simulation, we implemented the device structure as shown in Fig. 1 and calculated the dark current flowing in a one-pixel region. Detailed profiles for p-stops, sense nodes, BNWs, BPWs, and middle-Si layers were implemented based on the parameters provided by LAPIS Semiconductor Co. Ltd. In addition, it is generally known that the fixed positive charges are accumulated in the BOX layer during the wafer process. Therefore, we placed the fixed charge Q_{fix} of 2.0×10^{11} cm^{-2} uniformly between 1 and 3 nm above the Si/SiO$_2$ interface in reference to a previous study.[15]

We also implemented the radiation damage effects in the simulation. We reproduced the accumulation of positive charges by placing positive fixed charges Q_{BOX} in the BOX layer. We assumed that the concentration of Q_{BOX} increases in proportion to the dose based on the experimental results of a previous study.[5] In addition, to consider the carrier generation through the interface traps, we used the surface recombination model, expressed as[16]

$$U_{\text{SUR}} = \frac{n_i^2 - pn}{(n + n_i)/S_p + (p + n_i)/S_n} \quad (\text{cm}^{-2}/\text{s}), \tag{2}$$

where n_i is the intrinsic carrier density, p is the hole density, n is the electron density, and S is the surface recombination velocity. Subscripts p and n represent hole and electron, respectively. In this study, for the sake of simplification, we assume $S_n = S_p$. The surface recombination velocity is expressed as $S = \sigma v_{\text{th}} N_{\text{it}}$, where σ is the carrier capture cross section, v_{th} is the thermal velocity, and N_{it} is the interface state density.[16] We can calculate the carrier generation rate through the interface traps by applying this model to the Si/SiO$_2$ interface. According to a previous study,[17] N_{it} increases due to radiation damage, and thus the surface recombination velocity S must increase after x-ray irradiation. In Eq. (2), p and n are calculated by device simulation, and n_i is a constant. Therefore, because only $S_{n,p}$ is an unknown parameter and depends on the dose, it is necessary to model $S_{n,p}$ as a function of the dose based on the experimental results shown in Fig. 5(a).

To model $S_{n,p}$ as a function of the dose, we first need to reproduce the measured dark current in the simulation. Because the dark current is reproduced by the SUR [Eq. (2)] and Shockley–Read–Hall (SRH) models[16] in the simulation, the unknown parameters, $S_{n,p}$ in the SUR model and carrier lifetime $\tau_{n,p}$ in the SRH model, are adjusted. In HyDeLEOS, it is possible to adjust the carrier lifetime $\tau_{n,p}$ in the Si bulk by the coefficients of the carrier lifetimes of electrons (A_n) and holes (A_p) as

$$\tau_n = A_n \times \tau_{n0}, \quad \tau_p = A_p \times \tau_{p0}. \tag{3}$$

In this study, for the sake of simplification, we assumed $A_n = A_p$ and $S_n = S_p$. $\tau_{n0} \simeq 12.9$ μs and $\tau_{p0} \simeq 0.4$ μs are the fiducial values of the carrier lifetime defined as default parameters in HyDeLEOS for the sensor layer of XRPIX6C composed of p-type Si with a resistivity of 4 kΩ cm, which corresponds to the doping concentration of 3×10^{12} cm^{-3}.

To evaluate the reproducibility of the measured dark current by simulation, we calculated ΔI, which is the average value of the differences between the measured and simulated dark currents at multiple back-bias voltages V_{BB}. This takes into account the dark current generated from the sensor layer depleted by V_{BB}. Then, we adjusted the parameters $S_{n,p}$ and $A_{n,p}$ to minimize ΔI.
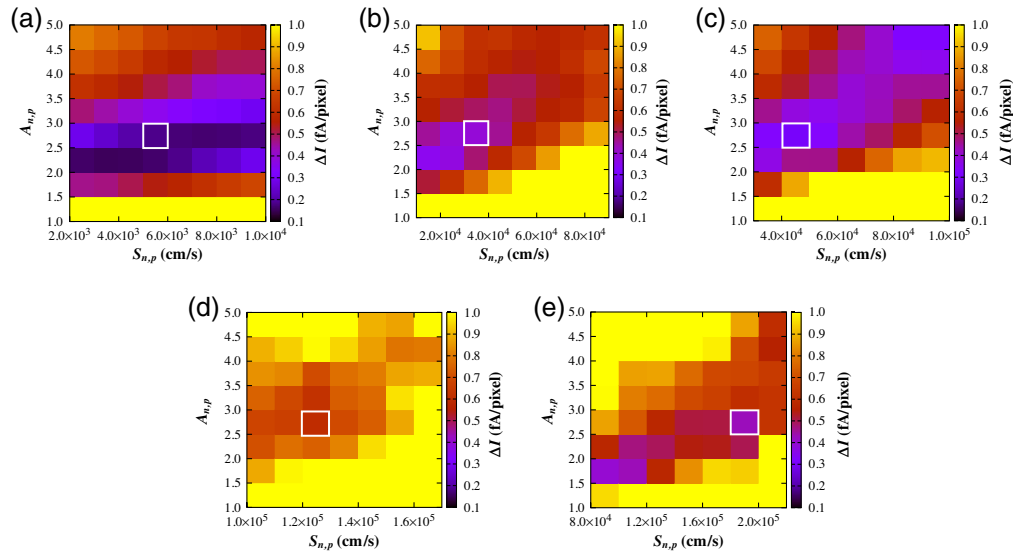
Fig. 9 The difference between the measured and simulated dark current ΔI as a function of the simulation parameters $S_{n,p}$ and $A_{n,p}$. The white squares indicate the best parameters, which have a lowest ΔI for each dose. (a) 0 rad, (b) 2 krad, (c) 4 krad, (d) 7 krad, and (e) 10 krad.

As shown in Fig. 9, the optimal values of $A_{n,p}$ do not change before and after radiation damage because the lattice defects in Si bulk, which shorten the carrier lifetime, do not increase due to x-ray irradiation in principle. The carrier lifetime $\tau_{n,p}$ remains at the same value ($\tau_n \simeq 30~\mu$s, $\tau_p \simeq 1~\mu$s) after 10-krad irradiation. These values are reasonable compared with those measured by the microwave-detected photoconductance decay method in a previous study.[18]

On the other hand, the optimal value of $S_{n,p}$ increased with increasing dose, as shown in Fig. 9. Then, we modeled the dependence of $S_{n,p}$ on the dose assuming a linear relationship between them. Figure 10 shows the optimal values of $S_{n,p}$ as a function of the dose, the best fit linear function, and its confidence intervals for 95% and 99%. As a result of linear fitting, slope 18.0 ± 2.1 cm $\cdot$ s^{-1} $\cdot$ rad^{-1} and intercept $(-7.6 \pm 1.2) \times 10^3$ cm/s were obtained as the best-fit parameters. According to the obtained linear model, the surface recombination velocity is $S_{n,p} \simeq 1.7 \times 10^5$ cm/s after 10-krad irradiation. This value of the surface recombination velocity is consistent with a previous study[19] for an irradiation of 10 krad.

Using the linear model of $S_{n,p}$ against the dose shown in Fig. 10, we compare the dose dependence of the measured dark current with the simulated dark current. Figure 11(a) shows
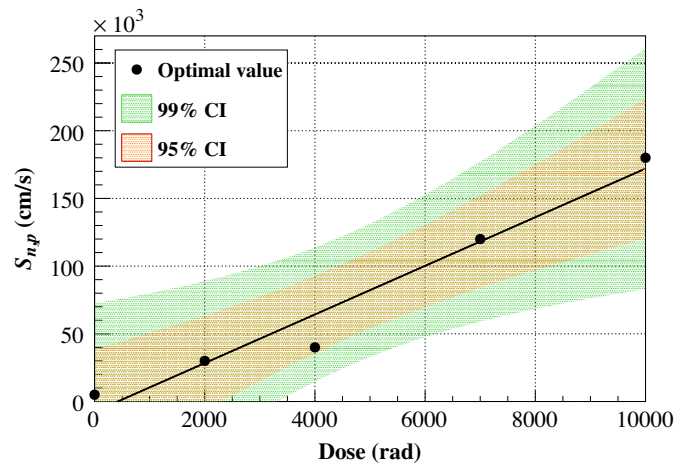

Fig. 10 The optimal values of $S_{n,p}$ as a function of dose level. The solid line indicates the best fit linear function. The shaded regions represent its confidence intervals of 95% and 99%.
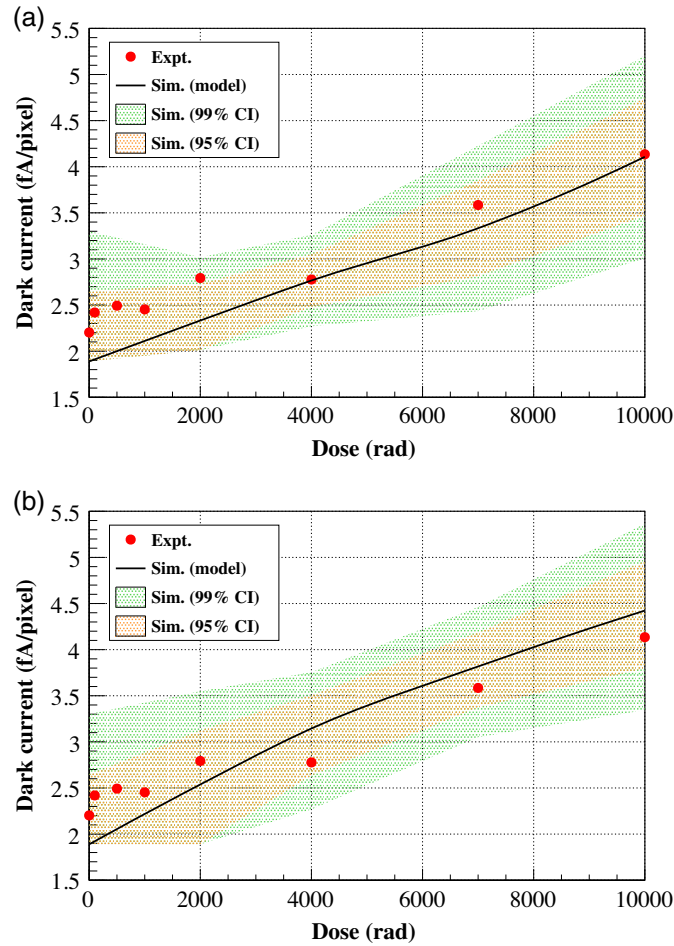
(a)

(b)

Fig. 11 Comparison of the experimental dark current degradation with the simulation in the cases (a) with Q_{BOX} and (b) without Q_{BOX}. The solid lines show the simulated dark current using the assumed linear model. The shaded regions show the simulated dark current using $S_{n,p}$ at the upper and lower limits of the confidence intervals for each dose in Fig. 10.

the comparison between the measured dark current and simulated dark current using the assumed linear model. The shaded regions show the simulation results corresponding to the confidence intervals for each dose in Fig. 10. However, because $S_{n,p}$ never takes negative values, $S_{n,p}$ at 0 rad of the linear model and the lower limits of the confidence intervals at 0 rad and 2 krad are set to 0 cm/s. As shown in Fig. 11(a), TCAD simulation successfully reproduced the experimental result by taking into account two radiation damage effects, i.e., accumulation of BOX charges and increase of interface traps.

To understand how the accumulated positive charge Q_{BOX} and the interface traps contribute to the dark current, we discriminate these effects. In Fig. 11(b), Q_{BOX} is not added for any doses. In both Figs. 11(a) and 11(b), the parameter $S_{n,p}$ increases approximately in proportion to the dose as shown in Fig. 10, and the simulated dark current tends to increase as the dose increases. Therefore, the increase in the interface traps contributes to the dark current increase.

Comparing Figs. 11(a) and 11(b), the simulated dark current in Fig. 11(a), which contains Q_{BOX} with different concentrations at each dose, is slightly lower than that in Fig. 11(b), which contains no Q_{BOX}. To reveal the physical mechanism of this difference, we focus on the electron density distribution near the Si/SiO$_2$ interface. Figures 12(a) and 12(b) show the electron density map around the BNW without Q_{BOX} and with Q_{BOX}, respectively. In the case without Q_{BOX} of Fig. 12(a), both ends of the BNW are depleted and the Si/SiO$_2$ interface is bare. On the other hand, in the case with Q_{BOX} of Fig. 12(b), the region of high electron density extends horizontally because the Q_{BOX} attracts electrons near the Si/SiO$_2$ interface. These electrons fill the
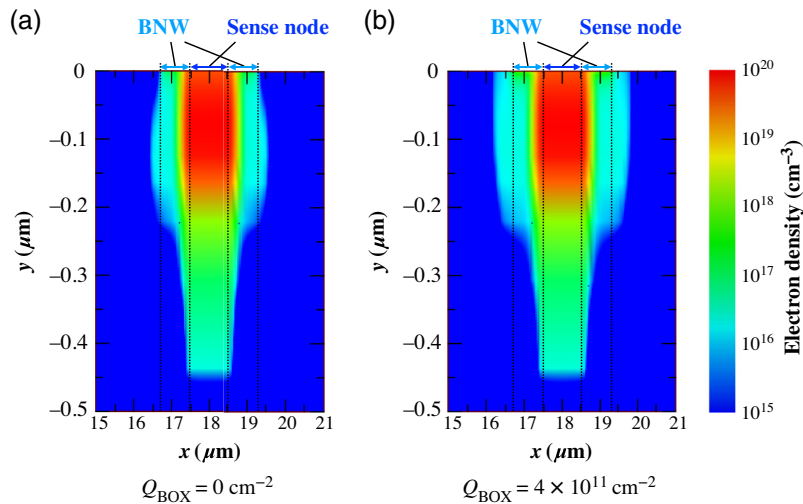
Fig. 12 The electron density distribution near the Si/SiO$_2$ interface ($y = 0$). (a) and (b) The cases with and without Q_{BOX}, respectively.

Si/SiO$_2$ interface, making it difficult for carriers to be generated, resulting in a lower dark current. Therefore, Q_{BOX} does not increase the dark current, but slightly decreases it.

5 Conclusion

We performed an irradiation experiment on D-SOI XRPIX using ∼10 keV x-rays with a total dose of 10 krad and investigated the physical mechanism of the degradation of detector performance. As the results, we found that the energy resolution at 5.9 keV x-ray degraded by 17.8% ± 2.8% and the dark current increased by 89% ± 13%. Especially regarding the dark current, we found that the increase in the interface trap density predominantly contributes to the increase in it. Moreover, the accumulated positive charge in the BOX layer does not increase the dark current. Thus, in the case of XRPIX and possibly the other SOI pixel sensors as well, it is important to reduce the dark current due to the interface traps to suppress the increase in dark current under the radiation environment.

Acknowledgments

References

1. K. Mori et al., "A broadband x-ray imaging spectroscopy with high-angular resolution: the FORCE mission," *Proc. SPIE* **9905**, 990510 (2016).
2. K. Nakazawa et al., "The FORCE mission: science aim and instrument parameter for broadband x-ray imaging spectroscopy with good angular resolution," *Proc. SPIE* **10699**, 106992D (2018).

3. T. G. Tsuru et al., "Kyoto's event-driven X-ray astronomy SOI pixel sensor for the FORCE mission," *Proc. SPIE* **10709**, 107090H (2018).

4. R. C. Hughes, "Hole mobility and transport in thin SiO_2 films," *Appl. Phys. Lett.* **26**, 436 (1975).

5. K. Hara et al., "Radiation hardness of silicon-on-insulator pixel devices," *Nucl. Instrum. Methods Phys. Res. Sect. A: Accel., Spectrom., Detect. Assoc. Equip.* **924**, 426–430 (2019).

6. K. Hagino et al., "Radiation damage effects on double-SOI pixel sensors for X-ray astronomy," *Nucl. Instrum. Methods Phys. Res. Sect. A: Accel., Spectrom., Detect. Assoc. Equip.* **978**, 164435 (2020).

7. K. Mori et al., "Total ionizing dose effects on the SOI pixel sensor for X-ray astronomical use," *Nucl. Instrum. Methods Phys. Res. Sect. A: Accel., Spectrom., Detect. Assoc. Equip.* **924**, 473–479 (2019).

8. M. Kitajima et al., "X-ray radiation damage effects on double-SOI pixel detectors for the future astronomical satellite," in *IEEE NSS/MIC Conf. Rec.* (2021).

9. Y. Arai et al., "Development of SOI pixel process technology," *Nucl. Instrum. Methods Phys. Res. Sect. A: Accel., Spectrom., Detect. Assoc. Equip.* **636**, S31–S36 (2011).

10. K. Hagino et al., "Sub-pixel response of double-SOI pixel sensors for X-ray astronomy," *J. Instrum.* **14**, C10023 (2019).

11. J. R. Schwank et al., "Radiation effects in MOS oxides," *IEEE Trans. Nucl. Sci.* **55**, 1833–1853 (2008).

12. S. Harada et al., "Performance of the silicon-on-insulator pixel sensor for X-ray astronomy, XRPIX6E, equipped with pinned depleted diode structure," *Nucl. Instrum. Methods Phys. Res. Sect. A: Accel., Spectrom., Detect. Assoc. Equip.* **924**, 468–472 (2019).

13. Y. Nemirovsky, I. Brouk, and C. Jakobson, "1/f noise in CMOS transistors for analog applications," *IEEE Trans. Electron Devices* **48**(5), 921–927 (2001).

14. "3D TCAD Simulator HyENEXSS ver. 8.5K," Keio University TCAD Research and Development Center (2019).

15. V. V. Afanas'ev and A. Stesmans, "Positive charging of thermal $SiO_2/(100)Si$ interface by hydrogen annealing," *Appl. Phys. Lett.* **72**, 79–81 (1998).

16. S. M. Sze, *Physics of Semiconductor Devices*, 2nd ed., Wiley, New York (1981).

17. J. Shi et al., "Radiation-induced charge trapping in Si-MOS capacitors with HfO_2/SiO_2 gate dielectrics," *Nuclear Instrum. Methods Phys. Res. Sec. B: Beam Interact. Mater. At.* **479**, 150–156 (2020).

18. D. Schroder, "Carrier lifetimes in silicon," *IEEE Trans. Electron Devices* **44**, 160–170 (1997).

19. A. M. Tonigan et al., "Impact of surface recombination on single-event charge collection in an SOI technology," *IEEE Trans. Nucl. Sci.* **68**, 305–311 (2021).

Masatoshi Kitajima is a master's student at Tokyo University of Science, Japan. He received his BS degree in physics from Tokyo University of Science in 2020. His current research interests focus on developments of x-ray SOI pixel detectors for the x-ray astronomical satellite.

Biographies of the other authors are not available.